A Rational Formulation of Thermal Circuit Models for Electrothermal Simulation—Part I: Finite Element Method

Jia Tzer Hsu and Loc Vu-Quoc

Abstract—**As the size of the semiconductor devices is getting smaller with advanced technology, self-heating effects in power semiconductor devices are becoming important. An electrothermal simulation of complete power electronic systems that include Si chips, thermal packages, and heat sinks is essential for an accurate analysis of the behavior of these systems. This paper presents a rational approach to construct thermal circuit networks equivalent to a discretization of the heat equation by the finite element method. Elemental thermal circuit networks are developed, which correspond to the linear and cubic Hermite elements in the 1-D case, to the triangular and rectangular elements in the 2-D case, and to the tetrahedral and cube elements in the 3-D case. These thermal circuit networks are to be connected to the electrical networks of power electronic systems to provide complete electrothermal models that can be conveniently used in any circuit simulator package. Verification examples are presented to demonstrate the accuracy of the proposed formulation.**

I. Introduction

SINCE THE SIZE of the semiconductor devices is becoming smaller with advanced technology, and since the electrical characteristics of power electronic circuits and devices are greatly influenced by the temperature distribution inside the semiconductor devices (self-heating effects), it is important to simulate the coupled electrical and thermal systems simultaneously. Because most of the nonlinear semiconductor device models are implemented in the circuit simulators such as SPICE [1] and SABER [2], it is advantageous to perform electrothermal simulations inside circuit simulators. In order to put the thermal effects into the circuit simulators, thermal circuit networks are needed. In [3] and [4], a finite difference method (FDM) was used to develop thermal models for electrothermal simulations. In this paper, we present a rational approach to construct thermal networks equivalent to a discretization of the heat equation by the finite element method (FEM).

It is remarked in [5] and [6] that the main advantages of the FEM are that conservation laws are exactly satisfied even by coarse approximations; it is easy to treat irregular geometries; the computational mesh can be graded to be fine in regions of rapid change; local mesh refinement is easier to implement than in the FDM; and higher order approximations are more readily constructed. Another major difference is that FDM is restricted to the so-called structured meshes, while FEM is suitable for unstructured meshes. It is well known that structured meshes require far more degrees of freedom for a given level of accuracy than unstructured meshes. One disadvantage of using FEM is the greater degree of programming complexity, which can be avoided by using these FEM-based circuit networks since analytical expressions of the circuit components are used. Using 1-D linear finite elements and lumped masses, it is found that thermal networks based on the FDM are simply special cases of the FEM-based thermal networks. FEM-based thermal networks can produce more accurate results based on the same number of mesh nodes, especially in the 2-D and 3-D problems. Moreover, higher-order finite element approximations can be applied for higher accuracy.

FDM, FEM, FVM (Finite Volume Method), and BEM (Boundary Element Method) are popularly employed to solve partial differential equations (PDE's). Actually, these methods can be viewed as particular cases of the Galerkin projection. FEM is not only used to solve PDE's, but also provides a natural way to solve circuit networks; in fact, circuit elements have been recognized as 0-D (or scalar) finite elements [7]. The ordinary differential equations (ODE's) by finite element (FE) formulation for circuit networks are the same as the nodal equations formulated in traditional circuit simulators. FE formulation can be modified so that results similar to the modified nodal equations [8] or the reduced modified nodal equations [9] can be obtained. Circuit techniques for solving PDE's have been widely discussed in the literature. Circuit technique for semiconductor analysis was proposed to solve semiconductor equations ([10], [11]). Retarded partial element equivalent circuit was used to solve transmission line problems [12]. Here, we derive the thermal networks based on a FE formulation for electrothermal simulations. Recently, FEM-based circuit models have been proposed for solving coupled field-circuit problems ([13], [14]); however, these models rely on the so-called mutual capacitors, mutual inductors, and mutual resistors. The present paper proposes a rational approach to construct thermal networks that do not use mutual capacitors/inductors/resistors.

The present FEM-based thermal networks are written as element templates in the SABER circuit simulator. It is convenient to represent a FE discretization in circuit simulators by treating one FE as one lumped circuit component. Accordingly, different types of finite elements are modeled as different types of lumped thermal circuit components. Model

Manuscript received February 7, 1995; revised July 25, 1995. This paper was recommended by Associate Editor M. K. Kazimierczuk.

The authors are with the Department of Aerospace Engineering, Mechanics and Engineering Science, University of Florida, Gainesville, FL 32611 USA.

Publisher Item Identifier S 1057-7122(96)06853-5.

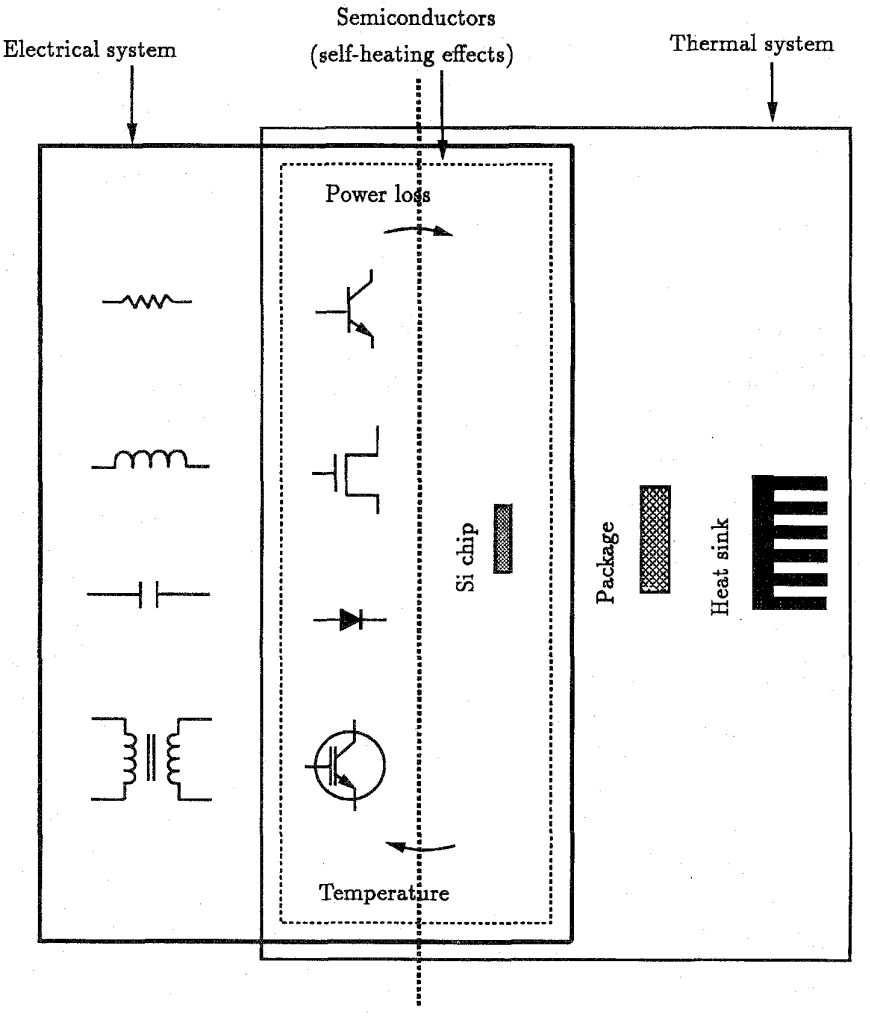

Fig. 1. Coupled electrothermal system.

reduction techniques to increase the simulation efficiency will be discussed in Part II of the present paper.

II. Coupled Electrothermal Equations

As shown in Fig. 1, self-heating effects of the semiconductor devices play important roles in the electrothermal simulation. Moreover, thermal packages, heat sinks, and other electrical components are also important for an accurate electrothermal simulation of power electronic circuits and devices. The nonlinear electrical system can be generally expressed as

$$\begin{aligned} \dot{\mathbf{u}} &= f(\mathbf{u}, \mathbf{e}, T) \\ \mathbf{P} &= \mathbf{P}(\mathbf{u}) \end{aligned} \tag{2.1}$$

where $\mathbf{u}$ is the vector containing nodal voltages or currents, $\mathbf{e}$ the electrical input (e.g., driving voltages for switches), T the temperature, and $\mathbf{P}$ the electrical power loss. The nonlinear electrical system is governed by the semiconductor equations (PDE's) and circuit equations (ODE's). The electrical power losses are originated from the heat generation inside the semiconductor devices. Since the semiconductor pn junction region, which results in most of the heat generation, is small compared to the whole device region, and is close to the top surface of the Si chip, the electrical power loss can be assumed to be imported from the top boundary of the Si chip, i.e., the electrical power loss is treated as a boundary condition in the thermal problem.

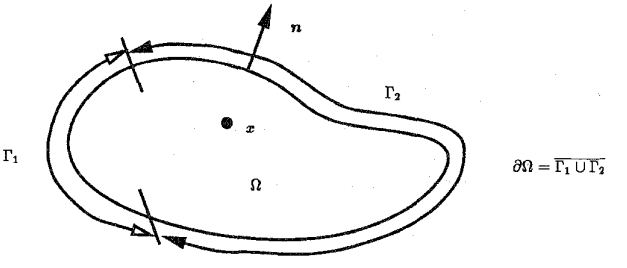

Fig. 2. Mathematical domain of the thermal problem.

The thermal system is governed by the partial differential equation

$$\operatorname{div}(\kappa \operatorname{grad} T) + g = \rho c_p \frac{\partial T}{\partial t} \quad \text{in } \Omega \tag{2.2}$$

with boundary conditions[1]

$$\kappa \operatorname{grad} T \cdot \mathbf{n} = \kappa \frac{\partial T}{\partial n} = \frac{P}{A} \quad \text{on } \Gamma_1 \tag{2.3}$$

$$\kappa \operatorname{grad} T \cdot \mathbf{n} = \kappa \frac{\partial T}{\partial n} = h(T_a - T) \quad \text{on } \Gamma_2 \tag{2.4}$$

and initial condition

$$T(x,0) = T_a = 300 \text{ K} \tag{2.5}$$

where $T: \Omega \times \Re_+ \to \Re$ is the temperature (a function of space and time), $g: \Omega \times \Re_+ \to \Re$ the generating heat, $\kappa: \Omega \to \Re$ the thermal conductivity, $\rho: \Omega \to \Re$ the mass density, $c_p: \Omega \to \Re$ the specific heat, $P: \Gamma_1 \times \Re_+ \to \Re$ the input power from boundary Γ_1, A the input power cross section area, h the convection coefficient, $\mathbf{n}$ the outward normal vector to the boundary, and T_a the ambient temperature. $\Re$ is the set of real numbers, $\Re_+ := \{t \in \Re \mid t \geq 0\}$, $\Omega \subset \Re^s$, where s is the number of space dimension, $s = 1$, 2, 3, and $\partial\Omega = \overline{\Gamma_1 \cup \Gamma_2}$ the closure of the union Γ_1 and Γ_2 (see, e.g., Hughes [1987]). The boundary condition on Γ_1 is derived from the first law of thermodynamics, and the convective boundary condition on Γ_2 is derived from the Newton's law of cooling.

The semidiscrete equation of (2.2)–(2.5), derived from a Galerkin finite element projection [15], is

$$\mathbf{M}\dot{d} + \mathbf{K}\mathbf{d} = \mathbf{F} \tag{2.6}$$

where $T(x,t) = \sum_{i=1}^{n} d_i(t) N_i(x)$—with $d_i(t)$ being the temperature at node i, and $N_i(x)$ being the associated FE basis function—$\mathbf{d}(t)$ the vector containing all nodal temperatures d_i's, and $\dot{\mathbf{d}}(t)$ the time derivative of $\mathbf{d}(t)$. The mass matrix $\mathbf{M}$ can be realized by capacitor elements, the stiffness matrix $\mathbf{K}$ by resistor elements, and the force vector $\mathbf{F}$ by current sources, so that thermal effects can be incorporated into circuit simulators. The global matrices $\mathbf{M}$, $\mathbf{K}$, and $\mathbf{F}$ are assembled from the elemental matrices $\mathbf{m}_e$, $\mathbf{k}_e$, and $\mathbf{f}_e$

$$\mathbf{M} = \bigoplus_{e=1}^{\text{nel}} \mathbf{m}_e, \quad \mathbf{K} = \bigoplus_{e=1}^{\text{nel}} \mathbf{k}_e, \quad \mathbf{F} = \bigoplus_{e=1}^{\text{nel}} \mathbf{f}_e \tag{2.7}$$

$$\mathbf{m}_e = [(m_e)_{ij}], \quad \mathbf{k}_e = [(k_e)_{ij}], \quad \mathbf{f}_e = [(f_e)_i]. \tag{2.8}$$

Expressions for the elements of the matrices $\mathbf{m}_e$, $\mathbf{k}_e$, and $\mathbf{f}_e$ are given below

$$(m_e)_{ij} = \rho c_p A \int_{\Omega_e} N_i N_j d\Omega_e \tag{2.9}$$

$$(k_e)_{ij} = \kappa A \int_{\Omega_e} \operatorname{grad} N_i \cdot \operatorname{grad} N_j d\Omega_e + hA \int_{\Gamma_2} N_i N_j d\Gamma_2 \tag{2.10}$$

$$(f_e)_i = P \int_{\Gamma_1} N_i d\Gamma_1 + hAT_a \int_{\Gamma_2} N_i d\Gamma_2 + A \int_{\Omega_e} g N_i d\Omega_e. \tag{2.11}$$

Equation (2.9) and the first term of (2.10) are the conductive terms. The second terms of (2.10) and (2.11) are the convective terms. The first and third terms of (2.11) are the input power and the heat generation terms, respectively. The thermal network based on FEM is an equivalent circuit network that yields the same semidiscrete system of (nonlinear) ODE's resulting from a Galerkin projection using, e.g., FE basis functions. Similar to FE global matrices, the global thermal network is assembled from elemental networks equivalent to the elemental matrices $\mathbf{m}_e$, $\mathbf{k}_e$, $\mathbf{f}_e$. Thus only elemental networks need to be considered.

[1]The convective boundary condition (2.4) can be used to approximate the Dirichlet boundary condition by choosing a large convective coefficient h. Since $\kappa \frac{\partial T}{\partial n}$ is finite, we have $T \to T_a$ as $h \to \infty$.

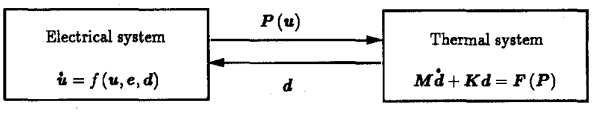

Fig. 3. Coupled electrothermal system.

In the circuit simulators, the linearized circuit equations of (2.1) are usually expressed as nodal equations

$$\mathbf{Y}(\mathbf{d})\mathbf{V} = \mathbf{I}$$

or modified nodal equations [16], where $\mathbf{V}$ is the vector of nodal voltages, $\mathbf{I}$ the vector of currents, and the admittance matrix $\mathbf{Y}$ is a function of temperatures $\mathbf{d}$. The coupled electrothermal system is shown in Fig. 3, from which it can be seen that the coupling between these two systems is based on the power losses $\mathbf{P}$ and the nodal temperatures $\mathbf{d}$. Note that d_i's in $\mathbf{d}$ are treated as system variables in the SABER circuit simulator, and the coupled electrical and thermal systems are solved simultaneously.

III. Background

A. FE Formulation for Circuit Elements

Fig. 4(a) shows two separated resistors which can be described by the following two equations

$$\begin{pmatrix} I_1 \\ I_2 \end{pmatrix} = \frac{1}{R_1} \begin{bmatrix} 1 & -1 \\ -1 & 1 \end{bmatrix} \begin{pmatrix} V_1 \\ V_2 \end{pmatrix}, \tag{3.1}$$

$$\begin{pmatrix} I_3 \\ I_4 \end{pmatrix} = \frac{1}{R_2} \begin{bmatrix} 1 & -1 \\ -1 & 1 \end{bmatrix} \begin{pmatrix} V_2 \\ V_3 \end{pmatrix}. \tag{3.2}$$

These two resistors and one external current source are assembled in Fig. 4(b), and the assembled system is described by

$$\begin{pmatrix} I_1 \\ I_{\text{ext}} \\ I_4 \end{pmatrix} = \begin{bmatrix} \frac{1}{R_1} & -\frac{1}{R_1} & 0 \\ -\frac{1}{R_1} & \frac{1}{R_1} + \frac{1}{R_2} & -\frac{1}{R_2} \\ 0 & -\frac{1}{R_2} & \frac{1}{R_2} \end{bmatrix} \begin{pmatrix} V_1 \\ V_2 \\ V_3 \end{pmatrix} \tag{3.3}$$

from which it can be seen that the basic rule of the FE assemblage for the circuit elements is the same as the Kirchhoff law, i.e., all currents flowing into the same node sum up to zero. Fig. 5 shows a general case (using resistors as an example), where the assemblage of the circuit elements is based on

$$\sum_{i=1}^{n} I_i = I_{\text{ext}}. \tag{3.4}$$

In the FE formulation, every circuit element such as a resistor, a capacitor, an inductor, and a current source is treated as one elemental matrix, and the connection of these circuit elements

is described by the assemblage of these elemental matrices. The matrix equations derived from the FE formulation for the circuit networks have the following form: ([7], [17])

$$\mathbf{M}\ddot{\mathbf{w}} + \mathbf{B}\dot{\mathbf{w}} + \mathbf{K}\mathbf{w} = \mathbf{F} \tag{3.5}$$

where $\dot{\mathbf{w}} = \mathbf{V}$ is the vector of nodal voltages, $\ddot{\mathbf{w}} = \dot{V} = d\mathbf{V}/dt$, and $\mathbf{w} = \int \mathbf{V}dt$. The global matrices $\mathbf{M}$, $\mathbf{B}$, and $\mathbf{K}$ are assembled from the local elemental matrices $\mathbf{m}_e$, $\mathbf{b}_e$, and $\mathbf{k}_e$, and the global vector $\mathbf{F}$ from the local elemental vector $\mathbf{f}_e$. If one of the element nodes is grounded, then the corresponding row and column in the global matrices will be eliminated. A capacitor element with a value C contributes to a local elemental matrix $\mathbf{m}_e$,

$$\mathbf{m}_e = \begin{bmatrix} 1 & -1 \\ -1 & 1 \end{bmatrix} C \tag{3.6}$$

a resistor element with a value R to a local elemental matrix $\mathbf{b}_e$,

$$\mathbf{b}_e = \begin{bmatrix} 1 & -1 \\ -1 & 1 \end{bmatrix} \left(\frac{1}{R}\right) \tag{3.7}$$

an inductor element with a value L to a local elemental matrix $\mathbf{k}_e$,

$$\mathbf{k}_e = \begin{bmatrix} 1 & -1 \\ -1 & 1 \end{bmatrix} \left(\frac{1}{L}\right) \tag{3.8}$$

and a current source element with a value I to a local elemental vector $\mathbf{f}_e$,

$$\mathbf{f}_e = \begin{pmatrix} I \\ -I \end{pmatrix}. \tag{3.9}$$

For a linearized h-parameter BJT (bipolar junction transistor) shown in Fig. 6, it will contribute to a local elemental matrix $\mathbf{b}_e$,

$$\mathbf{b}_e = \begin{bmatrix} \frac{h_{fe}}{h_{ie}} & h_{oe} - \frac{h_{fe}h_{re}}{h_{ie}} & -h_{oe} - \frac{h_{fe}(1-h_{re})}{h_{ie}} \\ \frac{1}{h_{ie}} & -\frac{h_{fe}}{h_{ie}} & -\frac{(1-h_{re})}{h_{ie}} \\ -\frac{h_{fe}}{h_{ie}} & -h_{oe} + \frac{h_{fe}h_{re}}{h_{ie}} & h_{oe} + \frac{h_{fe}(1-h_{re})}{h_{ie}} \end{bmatrix} \tag{3.10}$$

where the nodal sequence in $\mathbf{b}_e$ is collector, base, and emitter. The internal node x in the h-parameter BJT is eliminated by rudimentary manipulations. It is shown in [7] that this h-parameter BJT is handled by adding a one-ohm resistor into the model, so that FE formulation can be applied directly. Although it introduces a negligible error by adding this resistor, it is seen that $\mathbf{b}_e$ becomes a 5-by-5 matrix since the internal node is not eliminated and one more dimension is introduced by the added resistor. Since nodal equations are obtained through the FE formulation, a voltage source is not a natural element to be formulated into (3.5). Norton theorem is used in [7] to handle the voltage source with one grounded node. If the voltage source is connected to a circuit component other than the RLC lumped components, then a very small resistor need to be added to the network in order to apply the Norton theorem. This is similar to using a large penalty number in the FEM [18], [15]. The corresponding terms of the voltage source in (3.5) can be moved to the right-hand side and incorporated into the $\mathbf{F}$ vector. Accordingly, the nodes of the voltage sources are eliminated and extra current sources are added.

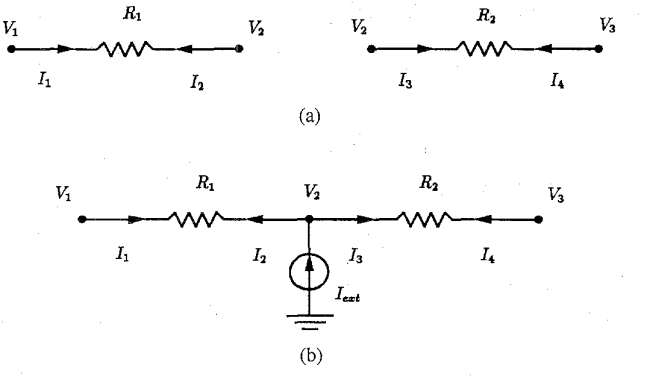

Fig. 4. (a) Two resistors before assemblage. (b) The assembled system of two resistors and one external current source.

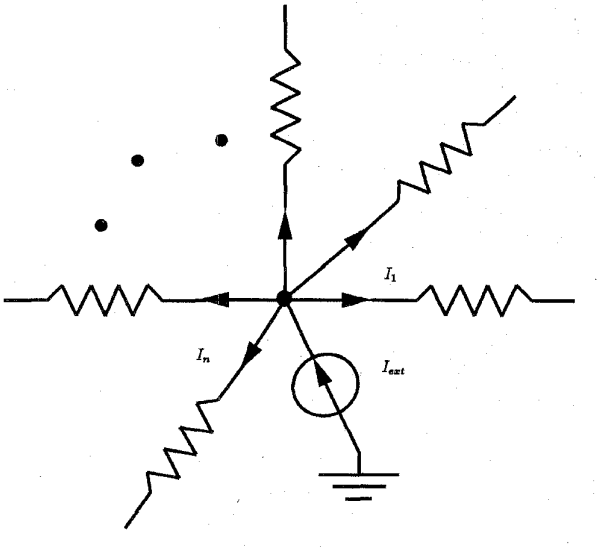

Fig. 5. A general example of circuit connection, using resistors as an example.

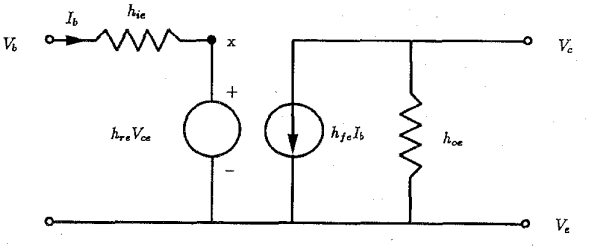

Fig. 6. h- parameter model of bipolar junction transistor.

B. Resemblance of Thermal and Circuit Systems

Fig. 7 shows a parallel RC circuit, which can be described by

$$C\begin{bmatrix} 1 & -1 \\ -1 & 1 \end{bmatrix}\begin{pmatrix} \dot{V}_1 \\ \dot{V}_2 \end{pmatrix} + \frac{1}{R}\begin{bmatrix} 1 & -1 \\ -1 & 1 \end{bmatrix}\begin{pmatrix} V_1 \\ V_2 \end{pmatrix} = \begin{pmatrix} I_1 \\ I_2 \end{pmatrix}. \tag{3.11}$$

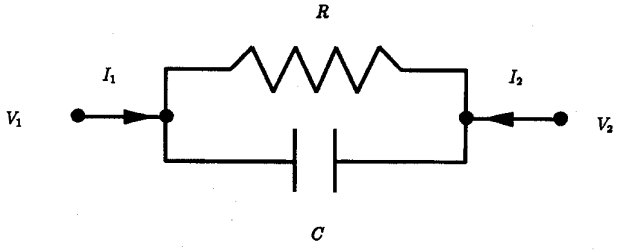

Fig. 7. A parallel RC circuit.

Comparing with the semidiscrete heat equation

$$\mathbf{M}\dot{\mathbf{d}} + \mathbf{K}\mathbf{d} = \mathbf{F} \tag{3.12}$$

it is easily seen that the mass matrix $\mathbf{M}$ can be realized by capacitor elements, the stiffness matrix $\mathbf{K}$ by resistor elements, and the force vector $\mathbf{F}$ by current sources. Some simple rules of obtaining the circuit networks from both the symmetric mass matrix and the symmetric stiffness matrix are discussed next.

C. Circuit Networks from Symmetric Matrices

Based on the above observation, a symmetric global matrix can be decomposed into several elemental matrices, and each elemental matrix can be represented by a circuit component. Some simple rules to obtain an equivalent circuit network from a symmetric matrix are summarized as follows. A symmetric mass matrix, $\mathbf{M} = [m_{ij}]$, can be realized by a capacitor network shown in Fig. 8, where

1) between node i and ground,

$$C_i = \sum_{j=1}^{n} m_{ij}. \tag{3.13}$$

2) between node i and node j,

$$C_{ij} = -m_{ij}. \tag{3.14}$$

A symmetric stiffness matrix, $\mathbf{K} = [k_{ij}]$, can be realized by a resistor network shown in Fig. 8, where

1) between node i and ground,

$$R_i = 1 \Big/ \left(\sum_{j=1}^{n} k_{ij} \right). \tag{3.15}$$

2) between node i and node j,

$$R_{ij} = -1/k_{ij}. \tag{3.16}$$

Thermal circuit networks by the Galerkin projection and model reduction techniques are derived from the above simple rules.

IV. Thermal Networks of 1-D Finite Elements

The length coordinate shown in Fig. 9 is used for the derivation of 1-D equivalent thermal networks. The length coordinates are written as

$$\begin{aligned} L_1 &= \frac{\text{length}(px_2^e)}{\text{length}(x_1^e x_2^e)} = \frac{x_2^e - x}{\delta_x}, \\ L_2 &= \frac{\text{length}(px_1^e)}{\text{length}(x_1^e x_2^e)} = \frac{x - x_1^e}{\delta_x}. \end{aligned} \tag{4.1}$$

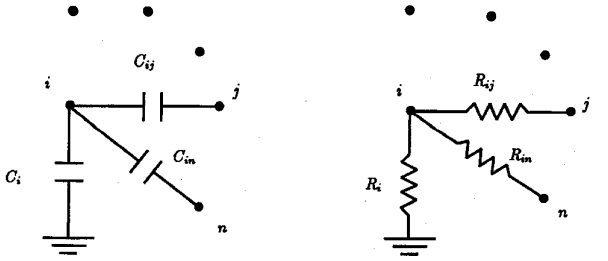

Fig. 8. A capacitor network from the symmetric mass matrix and a resistor network from the symmetric stiffness matrix.

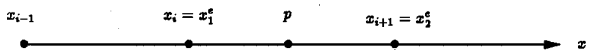

Fig. 9. Length coordinate.

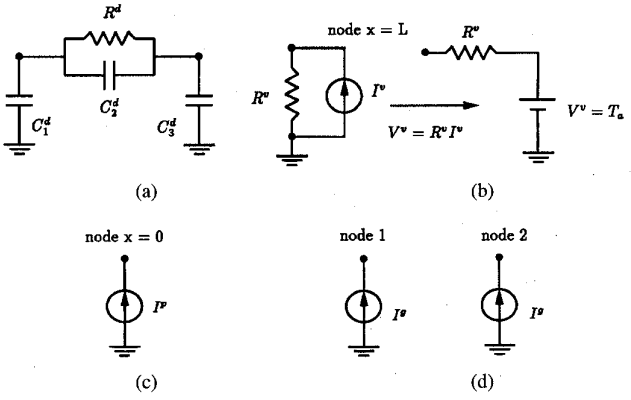

Fig. 10. 1-D linear element. (a) Conductive. (b) Convective. (c) Input power. (d) Heat generation thermal networks.

$(L_1, L_2) = (1, 0)$ at $x = x_1^e$, $(L_1, L_2) = (0, 1)$ at $x = x_2^e$, and $\delta_x = x_2^e - x_1^e$. Equations (2.9)–(2.11) in the 1-D problems can be calculated from the following formula [18]

$$\int_{\Omega_e} L_1^a L_2^b d\Omega_e = \frac{a!b!}{(a+b+1)!}\delta_x. \tag{4.2}$$

A. Thermal Network of 1-D Linear Element

For a 1-D linear element, basis functions and their derivatives in the length coordinate are

$$\begin{aligned} N_1(x) &= L_1, \quad N_2(x) = L_2, \\ N_{1,x}(x) &= \frac{-1}{\delta_x}, \quad N_{2,x}(x) = \frac{1}{\delta_x}. \end{aligned} \tag{4.3}$$

The conductive terms for the 1-D linear element are calculated to be

$$\mathbf{m}_e^d = \rho c_p A \delta_x \begin{bmatrix} \frac{1}{3} & \frac{1}{6} \\ \frac{1}{6} & \frac{1}{3} \end{bmatrix}, \quad \mathbf{k}_e^d = \frac{\kappa A}{\delta_x} \begin{bmatrix} 1 & -1 \\ -1 & 1 \end{bmatrix} \tag{4.4}$$

where the superscript d represents the conductive terms. From the simple rules discussed in Section III-C, the elemental

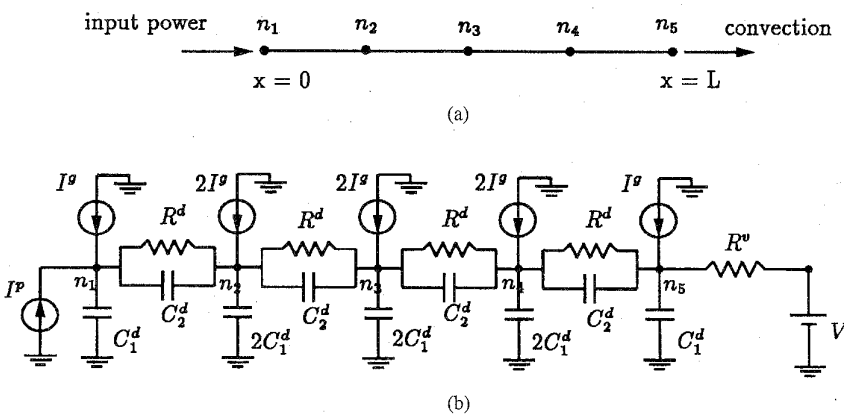

Fig. 11. (a) 1-D thermal problem and FE discretization. (b) Equivalent thermal network.

matrix $\mathbf{m}_e^d$ is realized by three capacitors

$$C_1^d = \left(m_e^d\right)_{11} + \left(m_e^d\right)_{12} = \frac{\rho c_p A \delta_x}{2},$$
$$C_2^d = -\left(m_e^d\right)_{12} = \frac{-\rho c_p A \delta_x}{6}, \tag{4.5}$$
$$C_3^d = \left(m_e^d\right)_{21} + \left(m_e^d\right)_{22} = \frac{\rho c_p A \delta_x}{2}$$

and the elemental matrix $\mathbf{k}_e^d$ by a resistor

$$R^d = -1/\left(k_e^d\right)_{12} = \frac{\delta_x}{\kappa A}. \tag{4.6}$$

Since $1/[(k_e^d)_{11} + (k_e^d)_{12}] = 1/[(k_e^d)_{21} + (k_e^d)_{22}] =$ infinite, there is no resistor between the two element nodes and ground. The equivalent conductive circuit network is shown in Fig. 10(a). For the element (last element for the 1-D case) with the convective boundary, we can write

$$\mathbf{m}_e = \mathbf{m}_e^d \bigoplus \mathbf{m}_e^v, \quad \mathbf{k}_e = \mathbf{k}_e^d \bigoplus \mathbf{k}_e^v, \quad \mathbf{f}_e = \mathbf{f}_e^g \bigoplus \mathbf{f}_e^v,$$
$$\mathbf{m}_e^v = 0, \quad \mathbf{k}_e^v = hA, \quad \mathbf{f}_e^v = hAT_a, \tag{4.7}$$
$$C^v = 0, \quad R^v = 1/hA, \quad I^v = hAT_a$$

where the superscript v represents the convective terms, and the superscript g represents the heat generation terms. The convective terms only exist at the end node ($x = L$). The second term in (2.10) is modeled by a resistor $R^v = 1/(hA)$, and the second term in (2.11) by a current source $I^v = hAT_a$. The equivalent convective thermal network is shown in Fig. 10(b), where the Thevenin theorem is applied to obtain an equivalent circuit. For the element (first element for the 1-D case) with the power input boundary, we can write

$$\mathbf{f}_e = \mathbf{f}_e^p \bigoplus \mathbf{f}_e^g,$$
$$\mathbf{f}_e^p = P \tag{4.8}$$

where the superscript p represents the power input terms. The input power only exists at the starting node ($x = 0$), and is modeled by a current source $I^p = P$. Internal heat generation exists at every element, and

$$\mathbf{f}_e^g = \frac{gA\delta_x}{2}\begin{pmatrix}1\\1\end{pmatrix}. \tag{4.9}$$

The uniform heat generation is modeled by two current sources $I^g = gA\delta_x/2$. The circuit networks for the input power and the uniform heat generation are shown in Fig. 10(c) and (d), respectively. Fig. 11 illustrates the assemblage of elemental thermal networks into a global one for a 1-D thermal problem. Capacitors C_2^d can be avoided if lumped mass is used instead of consistent mass [15].

B. Thermal Network of 1-D Cubic Hermite Element

The basis functions for a 1-D cubic Hermite element in the length coordinate are

$$N_1(x) = L_1^2(1 + 2L_2), \quad N_2(x) = L_1^2 L_2 \delta_x,$$
$$N_3(x) = (1 + 2L_1)L_2^2, \quad N_4(x) = -L_1 L_2^2 \delta_x. \tag{4.10}$$

The basis functions satisfy the following conditions:

1) at node 1 ($x = x_1^e$)

$$N_1 = \frac{dN_2}{dx} = 1,$$
$$\frac{dN_1}{dx} = N_2 = N_3 = \frac{dN_3}{dx} = N_4 = \frac{dN_4}{dx} = 0, \tag{4.11}$$

2) at node 2 ($x = x_2^e$)

$$N_3 = \frac{dN_4}{dx} = 1,$$
$$N_1 = \frac{dN_1}{dx} = N_2 = \frac{dN_2}{dx} = \frac{dN_3}{dx} = N_4 = 0, \tag{4.12}$$

3)

$$N_1 + N_3 = 1, \tag{4.13}$$

4)

$$N_1 x_1^e + N_2 + N_3 x_2^e + N_4 = x. \tag{4.14}$$

The conductive terms are calculated to be

$$\mathbf{m}_e^d = \rho c_p A \begin{bmatrix} \frac{13}{35}\delta_x & \frac{11}{210}\delta_x^2 & \frac{9}{70}\delta_x & \frac{-13}{420}\delta_x^2 \\ \frac{11}{210}\delta_x^2 & \frac{1}{105}\delta_x^3 & \frac{13}{420}\delta_x^2 & \frac{-1}{140}\delta_x^3 \\ \frac{9}{70}\delta_x & \frac{13}{420}\delta_x^2 & \frac{13}{35}\delta_x & \frac{-11}{210}\delta_x^2 \\ \frac{-13}{420}\delta_x^2 & \frac{-1}{140}\delta_x^3 & \frac{-11}{210}\delta_x^2 & \frac{1}{105}\delta_x^3 \end{bmatrix} \tag{4.15}$$

$$\mathbf{k}_e^d = \kappa A \begin{bmatrix} \frac{6}{5\delta_x} & \frac{1}{10} & \frac{-6}{5\delta_x} & \frac{1}{10} \\ \frac{1}{10} & \frac{2}{15}\delta_x & \frac{-1}{10} & \frac{-1}{30}\delta_x \\ \frac{-6}{5\delta_x} & \frac{-1}{10} & \frac{6}{5\delta_x} & \frac{-1}{10} \\ \frac{1}{10} & \frac{-1}{30}\delta_x & \frac{-1}{10} & \frac{2}{15}\delta_x \end{bmatrix}. \tag{4.16}$$

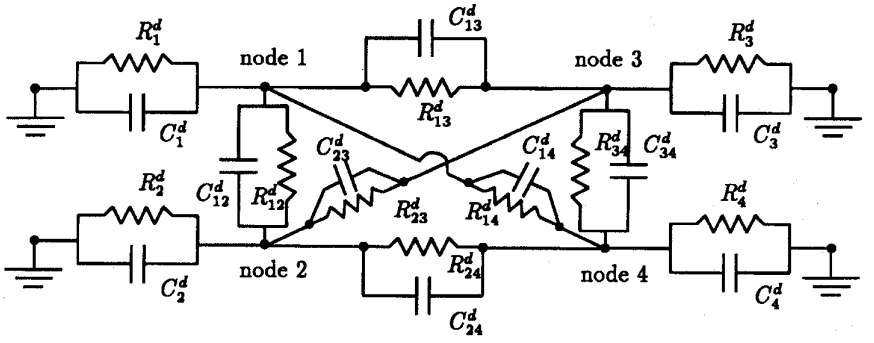

Fig. 12. Conductive thermal network for a 1-D cubic Hermite element.

The elemental conductive thermal network for the cubic Hermite element is shown in Fig. 12, where

$$
\begin{aligned}
&R_1^d = \frac{5}{\kappa A}, \quad R_2^d = \frac{10}{\kappa A \delta_x}, \quad R_3^d = \frac{-5}{\kappa A},\\
&R_4^d = \frac{10}{\kappa A \delta_x}, \quad R_{12}^d = \frac{-10}{\kappa A}, \quad R_{13}^d = \frac{5\delta_x}{6\kappa A},\\
&R_{14}^d = \frac{-10}{\kappa A}, \quad R_{23}^d = \frac{10}{\kappa A}, \quad R_{24}^d = \frac{30}{\kappa A \delta_x},\\
&R_{34}^d = \frac{10}{\kappa A}, \quad C_1^d = \rho c_p A\left(\frac{1}{2}\delta_x + \frac{3}{140}\delta_x^2\right),\\
&C_2^d = \rho c_p A\left(\frac{1}{420}\delta_x^3 + \frac{1}{12}\delta_x^2\right),\\
&C_3^d = \rho c_p A\left(\frac{1}{2}\delta_x - \frac{3}{140}\delta_x^2\right),\\
&C_4^d = \rho c_p A\left(\frac{1}{420}\delta_x^3 - \frac{1}{12}\delta_x^2\right), \quad C_{12}^d = \rho c_p A\left(\frac{-11}{210}\delta_x^2\right),\\
&C_{13}^d = \rho c_p A\left(\frac{-9}{70}\delta_x\right), \quad C_{14}^d = \rho c_p A\left(\frac{13}{420}\delta_x^2\right),\\
&C_{23}^d = \rho c_p A\left(\frac{-13}{420}\delta_x^2\right), \quad C_{24}^d = \rho c_p A\left(\frac{1}{140}\delta_x^3\right),\\
&C_{34}^d = \rho c_p A\left(\frac{11}{210}\delta_x^2\right).
\end{aligned}
\tag{4.17}
$$

Nodes 1, 3 give temperatures and nodes 2, 4 give temperature gradients. The convective terms and the input power term are modeled the same as those for the 1-D linear element. The uniform heat generation is modeled by three current sources. Two current sources with value $I_1^g = gA\delta_x/2$ are flowing from ground to node 1 and node 3, and one current source with value $I_2^g = gA\delta_x^2/12$ is flowing from node 4 to node 2.

V. Thermal Networks of 2-D Finite Elements

The area coordinate shown in Fig. 13 is used for the derivation of 2-D equivalent thermal networks of Lagrange-type triangular elements. The area coordinates are written as

$$\lambda_i = \frac{\text{area}(pjk)}{\text{area}(123)} = \frac{\alpha_i + \beta_i x + \gamma_i y}{2A_e} \tag{5.1}$$

$$\alpha_i = \left(x_j^e y_k^e - x_k^e y_j^e\right), \quad \beta_i = \left(y_j^e - y_k^e\right), \quad \gamma_i = \left(x_k^e - x_j^e\right) \tag{5.2}$$

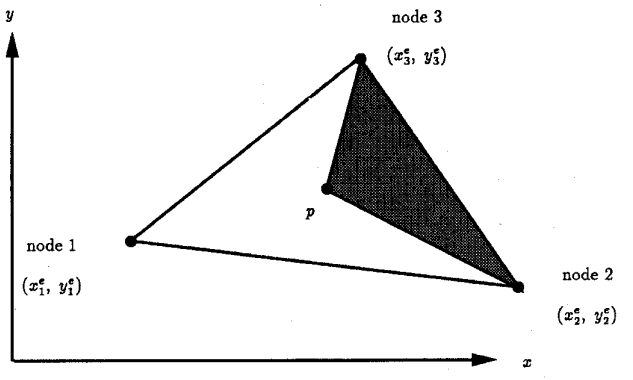

Fig. 13. Area coordinate.

where i, j, k are the cyclic permutation of 1, 2, 3, and A_e is the area of the local triangular element. Equations (2.9)–(2.11) in the 2-D problems can be calculated from the following formula [18]

$$\int_{\Omega_e} \lambda_1^a \lambda_2^b \lambda_3^c d\Omega_e = \frac{a!b!c!}{(a+b+c+2)!}(2A_e). \tag{5.3}$$

The coordinate transformation shown in Fig. 14 is used for the derivation of 2-D equivalent thermal networks of quadrilateral elements (with the rectangular element and the square element as special cases). Basis functions in the ξ-η coordinate are

$$N_i = \frac{1}{4}(1 + \xi_i\xi)(1 + \eta_i\eta), \quad i = 1 \text{ to } 4 \tag{5.4}$$

where ξ_i and η_i are either $+1$ or -1, and the following relations hold,

$$x(\xi,\eta) = \sum_{i=1}^{4} N_i(\xi,\eta)x_i^e, \quad y(\xi,\eta) = \sum_{i=1}^{4} N_i(\xi,\eta)y_i^e. \tag{5.5}$$

A. Thermal Network of 2-D Triangular Element

For a linear triangular element, basis functions in the area coordinate are

$$N_i(x,y) = \lambda_i, \quad i = 1,2,3. \tag{5.6}$$

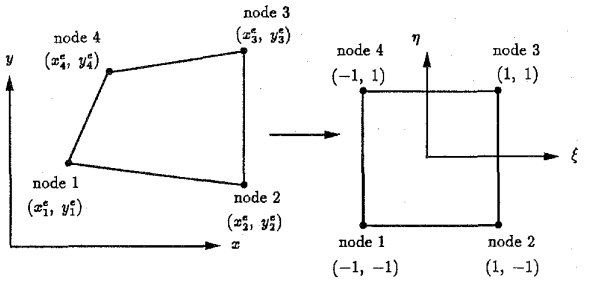

Fig. 14. Linear mapping from x-y coordinate to ξ-η coordinate.

The conductive terms are calculated to be

$$\mathbf{m}_e^d = \frac{\rho c_p A A_e}{12}\begin{bmatrix}2 & 1 & 1\\ 1 & 2 & 1\\ 1 & 1 & 2\end{bmatrix} \qquad \mathbf{k}_e^d = \frac{\kappa A}{4A_e}[k_{ij}], \quad i,j = 1 \text{ to } 3 \tag{5.7}$$

where $k_{ij} = \beta_i\beta_j + \gamma_i\gamma_j$. From the simple rules discussed in Section III-C, the elemental matrix $\mathbf{m}_e^d$ is modeled by three equal-valued capacitors $C_1^d = \rho c_p A A_e/3$, and by the other three equal-valued capacitors $C_2^d = -\rho c_p A A_e/12$. The elemental matrix $\mathbf{k}_e^d$ is modeled by three resistors connected among the element nodes

$$R_{ij}^d = \frac{-4A_e}{\kappa A(\beta_i\beta_j + \gamma_i\gamma_j)}, \quad 1 \le i < j \le 3. \tag{5.8}$$

No resistor is needed to connect the element nodes to ground, because the sum of those terms in the same row or column in $\mathbf{k}_e^d$ is zero. The signs of these three resistors depend on the corresponding triangular angles. An obtuse angle corresponds to a negative resistor, and a right angle to an infinite resistor which represents an open circuit. Otherwise, the corresponding resistor is positive. The elemental conductive thermal network is shown in Fig. 15(a). The convective terms are calculated to be

$$\mathbf{k}_e^v = hAL_{\Gamma_2}\begin{bmatrix}\frac{1}{3} & \frac{1}{6}\\ \frac{1}{6} & \frac{1}{3}\end{bmatrix}, \quad \mathbf{f}_e^v = \frac{hAT_aL_{\Gamma_2}}{2}\begin{bmatrix}1\\ 1\end{bmatrix} \tag{5.9}$$

where L_{Γ_2} is the length of the Γ_2 boundary line in a local triangular element. Similar to the 1-D conduction case, the elemental matrix $\mathbf{k}_e^v$ is modeled by two resistors $R_1^v = 2/(hAL_{\Gamma_2})$, and one resistor $R_2^v = -6/(hAL_{\Gamma_2})$. The vector $\mathbf{f}_e^v$ is modeled by two equal-valued current sources $I^v = hAT_aL_{\Gamma_2}/2$. The equivalent convective thermal network is shown in Fig. 15(b). The input power is modeled by two equal-valued current sources $I^p = PL_{\Gamma_1}/2$, where L_{Γ_1} is the length of the Γ_1 boundary line in a local triangular element. The uniform heat generation is modeled by three equal-valued current sources $I^g = gAA_e/3$. The circuit networks for the input power and the heat generation are shown in Figs. 15(c) and (d), respectively.

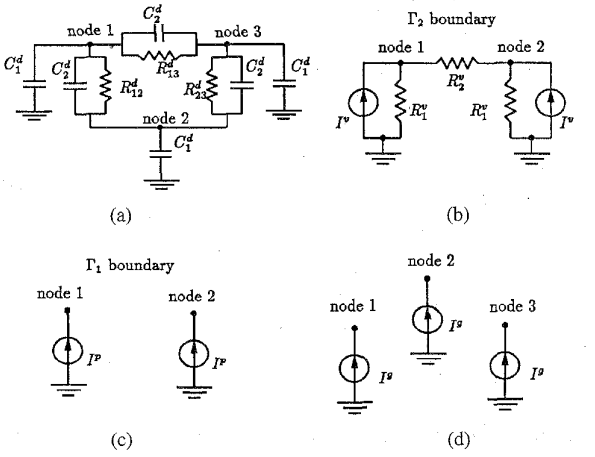

Fig. 15. 2-D triangular element: (a) Conductive. (b) Convective. (c) Input power. (d) Heat generation thermal networks.

B. Thermal Network of 2-D Rectangular (or Square) Element

Basis functions for the 2-D rectangular (or square) element are shown in (5.4). The conductive terms are calculated to be

$$\mathbf{m}_e^c = \frac{\rho c_p A\delta_x\delta_y}{36}\begin{bmatrix}4 & 2 & 1 & 2\\ 2 & 4 & 2 & 1\\ 1 & 2 & 4 & 2\\ 2 & 1 & 2 & 4\end{bmatrix} \tag{5.10}$$

and (5.11) shown at the bottom of the next page where δ_x and δ_y are the length and the width of the rectangular element, respectively. The conductive thermal network is shown in Fig. 16, where

$$C_1^d = \frac{1}{4}\rho c_p A\delta_x\delta_y, \quad C_2^d = \frac{-1}{18}\rho c_p A\delta_x\delta_y,$$
$$C_3^d = \frac{-1}{36}\rho c_p A\delta_x\delta_y,$$
$$R_1^d = \frac{6}{\kappa A\left(\frac{2\delta_x}{\delta_y} - \frac{\delta_y}{\delta_x}\right)}, \quad R_2^d = \frac{6}{\kappa A\left(-\frac{\delta_x}{\delta_y} + \frac{2\delta_y}{\delta_x}\right)}$$
$$R_3^d = \frac{6}{\kappa A\left(\frac{\delta_x}{\delta_y} + \frac{\delta_y}{\delta_x}\right)}. \tag{5.12}$$

For a square element, set $\delta_x = \delta_y = \delta$. The condition for R_1^d and R_2^d to be positive is

$$\frac{1}{\sqrt{2}} < \frac{\delta_x}{\delta_y} < \sqrt{2}. \tag{5.13}$$

Circuit models for the convective terms and the input power are the same as those for the 2-D linear triangular element. The uniform heat generation is modeled by four equal-valued current sources, $I^g = gA\delta_x\delta_y/4$.

VI. Thermal Networks of 3-D Finite Elements

The volume coordinate shown in Fig. 17 is used for the derivation of 3-D equivalent thermal networks of Lagrange-type tetrahedral elements. The volume coordinates are written as

$$V_i = \frac{\text{volume}(pjkl)}{\text{volume}(1234)} = \frac{\alpha_i + \beta_i x + \gamma_i y + \zeta_i z}{6V_e} \tag{6.1}$$

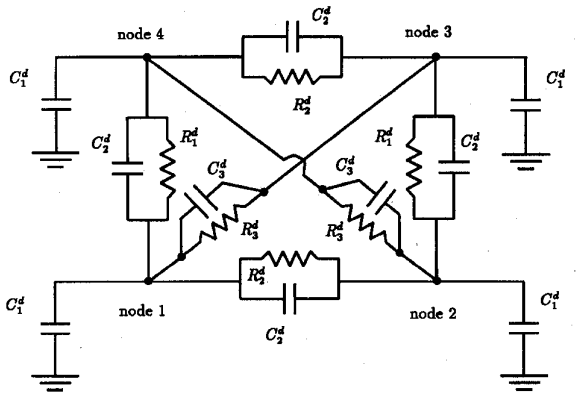

Fig. 16. Conductive thermal network for a 2-D rectangular element.

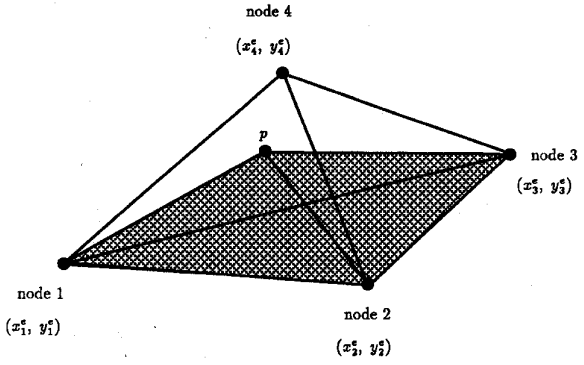

Fig. 17. Volume coordinate.

where i, j, k, l are the cyclic permutation of 1, 2, 3, 4, V_e is the volume of the local tetrahedral element, and $\alpha_i, \beta_i, \gamma_i, \zeta_i, i = 1$ to 4, can be found in [18]. Note that the ordering of the nodal numbers must follow a right-hand rule. Equations (2.9)–(2.11) in the 3-D problems can be calculated from the following formula [18]

$$\int_{\Omega_e} V_1^a V_2^b V_3^c V_4^d \, d\Omega_e = \frac{a!b!c!d!}{(a+b+c+d+3)!}(6V_e). \quad (6.2)$$

A. Thermal Network of 3-D Tetrahedral Element

For a linear tetrahedral element, basis functions in the volume coordinate are

$$N_i(x, y, z) = V_i, \quad i = 1 \text{ to } 4. \quad (6.3)$$

The conductive terms are calculated to be

$$\mathbf{m}_e^d = \frac{\rho c_p A V_e}{20}\begin{bmatrix} 2 & 1 & 1 & 1 \\ 1 & 2 & 1 & 1 \\ 1 & 1 & 2 & 1 \\ 1 & 1 & 1 & 2 \end{bmatrix}$$
$$\mathbf{k}_e^d = \frac{\kappa A}{36V_e}[k_{ij}], \quad i, j = 1 \text{ to } 4 \quad (6.4)$$

where $k_{ij} = \beta_i\beta_j + \gamma_i\gamma_j + \zeta_i\zeta_j$. The conductive thermal network is shown in Fig. 18(a), where

$$C_1^d = \frac{\rho c_p A V_e}{4}, \quad C_2^d = \frac{-\rho c_p A V_e}{20},$$
$$R_{ij}^d = \frac{-36V_e}{\kappa A(\beta_i\beta_j + \gamma_i\gamma_j + \zeta_i\zeta_j)}, \quad 1 \le i < j \le 4. \quad (6.5)$$

The convective terms are calculated to be

$$\mathbf{k}_e^v = \frac{hAA_{e,\Gamma_2}}{12}\begin{bmatrix} 2 & 1 & 1 \\ 1 & 2 & 1 \\ 1 & 1 & 2 \end{bmatrix},$$
$$\mathbf{f}_e^v = \frac{hAA_{e,\Gamma_2}T_a}{3}\begin{bmatrix} 1 \\ 1 \\ 1 \end{bmatrix} \quad (6.6)$$

where A_{e,Γ_2} is the area of the Γ_2 boundary surface in a tetrahedral element. The convective thermal network is shown in Fig. 18(b), where

$$R_1^v = \frac{3}{hAA_{e,\Gamma_2}}, \quad R_2^v = \frac{-12}{hAA_{e,\Gamma_2}}, \quad I^v = \frac{hAA_{e,\Gamma_2}T_a}{3}. \quad (6.7)$$

The input power is modeled by three equal-valued current sources $I^p = A_{e,\Gamma_1}P/3$, where A_{e,Γ_1} is the area of the Γ_1 boundary surface in a local tetrahedral element, and the uniform heat generation is modeled by four equal-valued current sources $I^g = gAV_e/4$. The circuit networks for the input power and the heat generation are shown in Fig. 18(c) and (d), respectively.

B. Thermal Network of 3-D Cube Element

Since the 3-D conductive thermal network is too complicated to draw here, node 1 in Fig. 19(a) is used as a reference node to illustrate the connections. The conductive terms for the cube element are modeled by 16 resistors and 36 capacitors. Only eight capacitors are needed if lumped mass is used instead of consistent mass. Resistors among the neighboring nodes, such as nodes 2, 4, 5 to node 1, are infinite and therefore are open. Sixteen resistors among the nonneighboring nodes, such as nodes 3, 6, 7, 8 to node 1,

$$\mathbf{k}_e^c = \frac{\kappa A}{6}\begin{bmatrix} 2\left(\frac{\delta_x}{\delta_y}+\frac{\delta_y}{\delta_x}\right) & \left(\frac{\delta_x}{\delta_y}-\frac{2\delta_y}{\delta_x}\right) & \left(-\frac{\delta_x}{\delta_y}-\frac{\delta_y}{\delta_x}\right) & \left(-\frac{2\delta_x}{\delta_y}+\frac{\delta_y}{\delta_x}\right) \\ \left(\frac{\delta_x}{\delta_y}-\frac{2\delta_y}{\delta_x}\right) & 2\left(\frac{\delta_x}{\delta_y}+\frac{\delta_y}{\delta_x}\right) & \left(-\frac{2\delta_x}{\delta_y}+\frac{\delta_y}{\delta_x}\right) & \left(-\frac{\delta_x}{\delta_y}-\frac{\delta_y}{\delta_x}\right) \\ \left(-\frac{\delta_x}{\delta_y}-\frac{\delta_y}{\delta_x}\right) & \left(-\frac{2\delta_x}{\delta_y}+\frac{\delta_y}{\delta_x}\right) & 2\left(\frac{\delta_x}{\delta_y}+\frac{\delta_y}{\delta_x}\right) & \left(\frac{\delta_x}{\delta_y}-\frac{2\delta_y}{\delta_x}\right) \\ \left(-\frac{2\delta_x}{\delta_y}+\frac{\delta_y}{\delta_x}\right) & \left(-\frac{\delta_x}{\delta_y}-\frac{\delta_y}{\delta_x}\right) & \left(\frac{\delta_x}{\delta_y}-\frac{2\delta_y}{\delta_x}\right) & 2\left(\frac{\delta_x}{\delta_y}+\frac{\delta_y}{\delta_x}\right) \end{bmatrix} \quad (5.11)$$

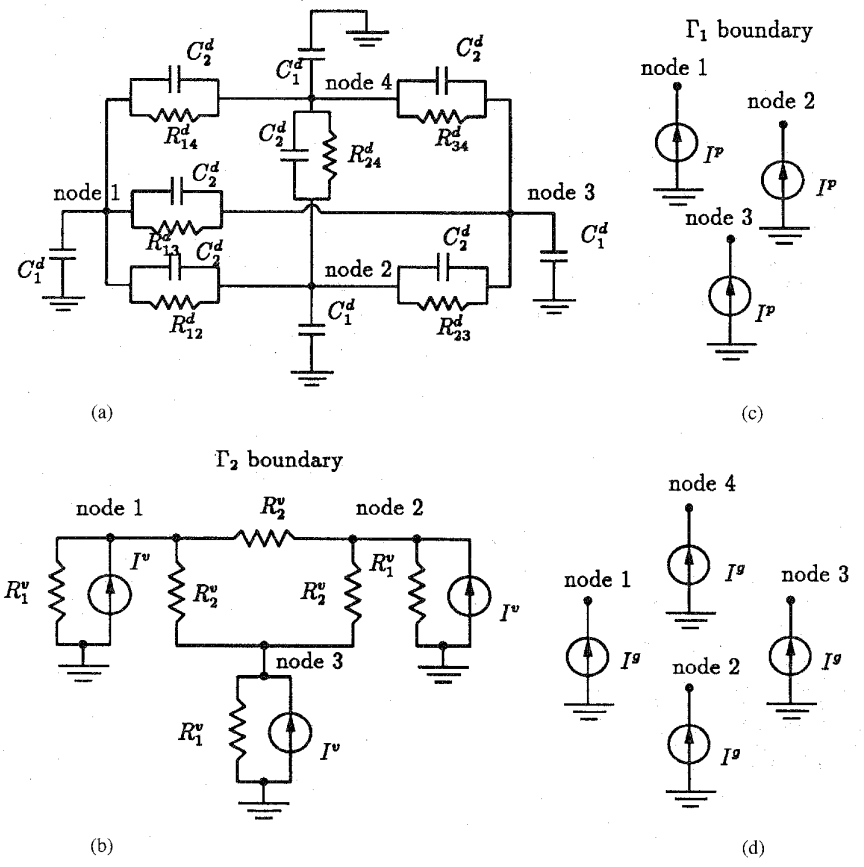

Fig. 18. 3-D tetrahedral element: (a) Conductive. (b) Convective. (c) Input power. (d) Heat generation thermal networks.

have the value $R^d = \kappa A\delta/12$, where δ is the length of the cube element. Eight equal-valued capacitors $C_1^d = \rho c_p A\delta^3/8$ connect the eight element nodes to ground. Twelve equal-valued negative capacitors $C_2^d = -\rho c_p A\delta^3/54$ are connected among the neighboring nodes, such as nodes 2, 4, 5 to node 1, twelve equal-valued negative capacitors $C_3^d = -\rho c_p A\delta^3/108$ are connected among the 2-D-diagonal nodes, such as nodes 3, 6, 8 to node 1, and four equal-valued capacitors $C_4^d = -\rho c_p A\delta^3/216$ are connected among the 3-D-diagonal nodes, such as node 7 to node 1. The convective terms are calculated to be

$$\mathbf{k}_e^v = \frac{hA\delta^2}{36}\begin{bmatrix}4 & 2 & 1 & 2\\ 2 & 4 & 2 & 1\\ 1 & 2 & 4 & 2\\ 2 & 1 & 2 & 4\end{bmatrix}$$
$$\mathbf{f}_e^v = \frac{hAT_a\delta^2}{4}\begin{pmatrix}1\\1\\1\\1\end{pmatrix}. \tag{6.8}$$

The equivalent convective thermal network is shown in Fig. 19(b), where

$$R_1^v = \frac{4}{hA\delta^2}, \quad R_2^v = \frac{-18}{hA\delta^2},$$
$$R_3^v = \frac{-36}{hA\delta^2}, \quad I^v = \frac{hAT_a\delta^2}{4}. \tag{6.9}$$

The input power is modeled by four equal-valued current sources $I^p = P\delta^2/4$, and the uniform heat generation by eight equal-valued current sources $I^g = gA\delta^3/8$. Capacitors C_2^d, C_3^d and C_4^d can be avoided if lumped mass is used instead of consistent mass.

VII. Verification

FEM-based thermal networks are written as element templates in the SABER circuit simulator, and thermal package models are built by these element templates. A nonlinear resistor template is used to account for the nonlinear thermal conductivity of silicon [4], i.e.,

$$\kappa(T) = 1.5486\left(\frac{300}{T}\right)^{\frac{4}{3}}. \tag{7.1}$$

A 2-D mesh generator is used to produce a mesh of triangular elements, and programs are written to automatically generate SABER input files. The coupled electrical and thermal systems are solved simultaneously by the built-in numerical solvers in SABER. The thermal circuit networks for the 1-D FE's are verified by analytical solutions for linear problems; the results are shown in Figs. 20 and 21. Using the method of separation of variables [19], the analytical solution

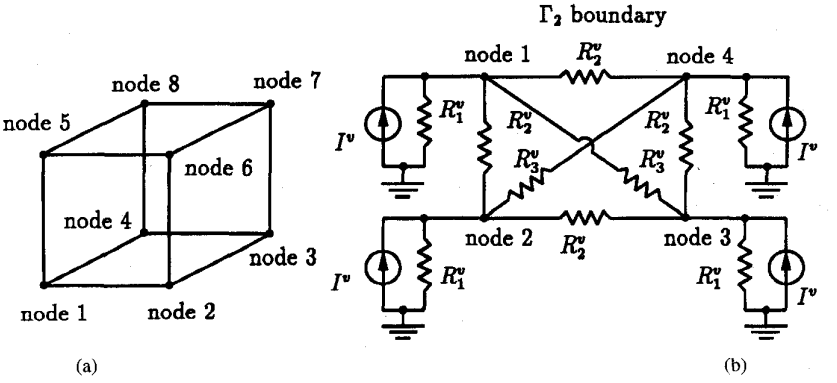

Fig. 19. (a) A cube element. (b) Convective thermal network for a cube element.

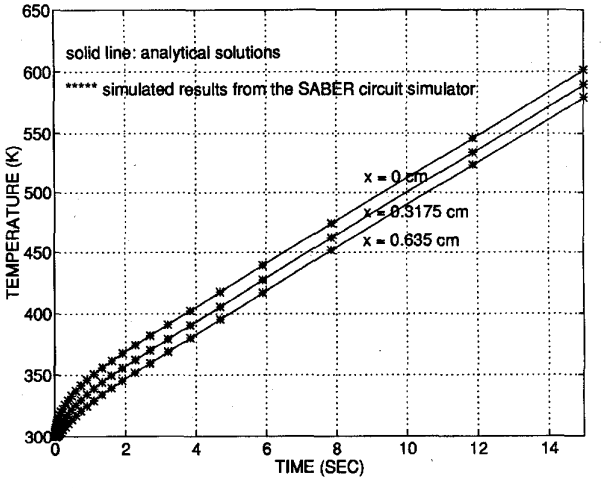

Fig. 20. Verification of 1-D thermal circuit networks: $h = 1.55 \times 10^{-3}$ W/cm^2-K.

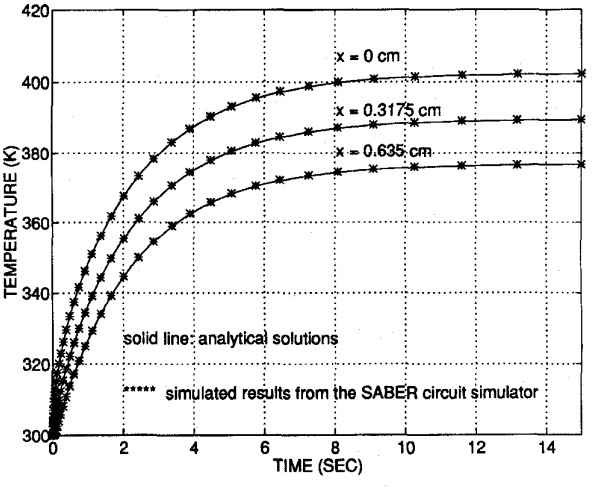

Fig. 21. Verification of 1-D thermal circuit networks: $h =$ infinite.

for the 1-D thermal problem is derived as[2]

$$T(x,t) = \frac{P}{\kappa A}(1-x) + \frac{P}{hA} + T_a + \sum_{n=1}^{\infty} D_n \exp\left(\frac{-\kappa}{\rho c_p}\lambda_n^2 t\right)\cos(\lambda_n x) \quad (7.2)$$

where λ_n satisfies

$$\lambda_n \tan(\lambda_n) = \frac{h}{\kappa} \quad (7.3)$$

and

$$D_n = \frac{4P\{h[\cos(\lambda_n) - 1] - \kappa\lambda_n \sin(\lambda_n)\}}{\kappa h \lambda_n A[2\lambda_n + \sin(2\lambda_n)]}. \quad (7.4)$$

The tested 1-D problem is shown in Fig. 11(a); the parameters used are: $\kappa = 3.846$ W/K-cm, $\rho = 8.857$ g/cm^3, $c_p = 0.386$ J/g-K, $P = 100$ W, $A = 0.645\,16$ cm^2, $L = 2.54$ cm, and element number = 8. The tested 2-D problem which only consists of the Si chip and the TO247 package, taken from a reference paper [4], is shown in Fig. 22. The thermal networks for the 2-D FE's are verified by results from the ANSYS[3] simulator; the results are shown in Fig. 23. Simulation results from SABER and from ANSYS are similar.

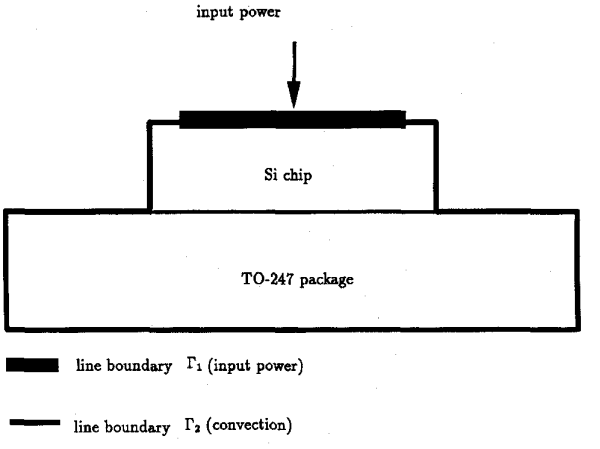

Fig. 22. One example of 2-D thermal problems.

[2] Only six terms, which can be obtained from [19], of the infinite series in (7.2) are used to produce the analytical solutions shown in Figs. 20 and 21.

[3] ANSYS is a FE program to solve PDE's, not a circuit simulator. We use ANSYS results to verify our FEM-based thermal circuit models developed for SABER, which is a circuit simulator.

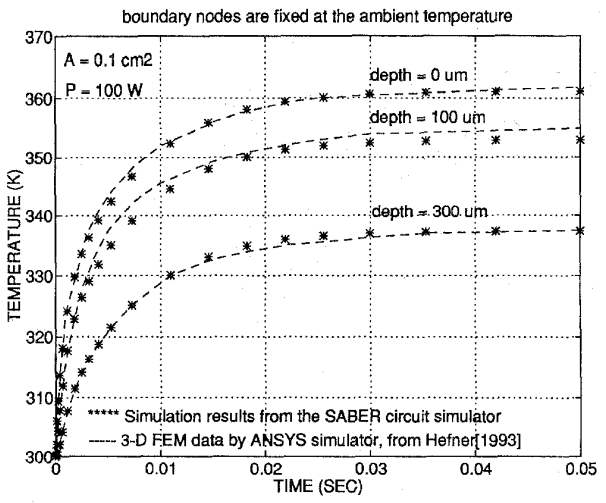

Fig. 23. Verification of 2-D thermal circuit networks.

VIII. Closure

A rational formulation of the thermal circuit networks by the finite element method has been presented. These FEM-based thermal circuit networks are implemented in the SABER circuit simulator, and simulation results are verified with the analytical solutions for the 1-D case, and by the results from a FEM code for the 2-D case. Different types of finite elements are modeled as different types of lumped thermal circuit components, so that finite element solutions of the thermal system are ready to be coupled with the electrical system in the electrothermal simulation.

Acknowledgment

The authors would like to thank K. D. T. Ngo for his support and discussions.

References

[1] P. W. Tuinenga, *SPICE—A Guide to Circuit Simulation & Analysis Using PSPICE*. Englewood Cliffs, NJ: Prentice Hall, 1988.
[2] Analogy Inc., Beaverton Oregon, *SABER User's Guide*, 3.1a ed., 1992.
[3] K. Fukahori and P. R. Gray, "Computer simulation of integrated circuits in the presence of electrothermal interaction," *IEEE J. Solid-State Circuits*, vol. SC-11, pp. 834–846, Dec. 1976.
[4] A. R. Hefner and D. L. Blackburn, "Simulating the dynamic electrothermal behavior of power electronic circuits and systems," *IEEE Trans. Power Electron.*, vol. 8, pp. 376–385, Oct. 1993.
[5] J. J. Barnes and R. J. Lomax, "Finite element methods in semiconductor device simulation," *IEEE Trans. Electron Devices*, vol. ED-34, pp. 1082–1088, Aug. 1977.
[6] R. Dautray and J. L. Lions, *Mathematical Analysis and Numerical Methods for Science and Technology*. New York: Springer-Verlag, 1990.
[7] J. R. Brauer, B. E. MacNeal, L. A. Larkin, and V. D. Overbye, "New method of modeling electronic circuits coupled with 3-D electromagnetic finite element models," *IEEE Trans. Magn.*, vol. 27, pp. 4085–4088, Sept. 1991.
[8] C. W. Ho, A. E. Ruehli, and P. A. Brennan, "The modified nodal approach to network analysis," *IEEE Trans. Circuits Syst.*, vol. CAS-22, pp. 504–509, June 1975.
[9] K. Lee and S. B. Park, "Reduced modified nodal approach to circuit analysis," *IEEE Trans. Circuits Syst.*, vol. CAS-32, pp. 1056–1060, Oct. 1985.
[10] C. T. Sah, "The equivalent circuit model in solid-state electronics—III," *IEEE J. Solid-State Circuits*, vol. 13, pp. 1547–1575, 1970.
[11] F. A. Lindholm and C. T. Sah, "Circuit technique for semiconductor-device analysis with junction diode open circuit voltage decay example," *IEEE J. Solid-State Circuits*, vol. 31, pp. 197–204, 1988.
[12] H. Heeb and A. E. Ruehli, "Three-dimensional interconnect analysis using partial elemental equivalent circuits," *IEEE Trans. Circuits Syst.*, vol. 39, pp. 974–982, Nov. 1992.
[13] I. A. Tsukerman, A. Konrad, and J. C. Sabonnadiere, "Coupled field-circuit problems: Trends and accomplishments," *IEEE Trans. Magn.*, vol. 29, pp. 1701–1704, Mar. 1993.
[14] A. Demenko, "Equivalent *RC* network with mutual capacitances for electromagnetic field simulation of electrical machine transients," *IEEE Trans. Magn.*, vol. 28, pp. 1406–1409, Mar. 1992.
[15] T. J. R. Hughes, *The Finite Element Method*. Englewood Cliffs, NJ: Prentice-Hall, 1987.
[16] W. J. McCalla, *Fundamentals of Computer-Aided Circuit Simulation*. Boston, MA: Kluwer Academic, 1988.
[17] R. H. V. Heiden, A. A. Arkadan, J. R. Brauer, and G. T. Hummert, "Finite element modeling of a transformer feeding a rectified load: The coupled power electronics and nonlinear magnetic field problem," *IEEE Trans. Magn.*, vol. 27, pp. 5217–5219, Nov. 1991.
[18] O. C. Zienkiewicz and R. L. Taylor, *The Finite Element Method*, 4th ed. New York: McGraw-Hill, vol. 1, 1989.
[19] M. N. Ozisik, *Heat Conduction*. New York: Wiley, 1980.

Jia-Tzer Hsu received the B.S. degree in electrical engineering from the National Cheng-Kung University, Taiwan, in 1984, and the M.S. degree in electrical engineering from the University of Florida, Gainesville, in 1990. He also received a second M.S. degree in engineering mechanics from a concurrent degree program at the University of Florida, in 1994.

He is currently completing the Ph.D. degree in electrical engineering. His Ph.D. work focuses on the development of CAD models and the formulations for electro/magnetothermal simulations of power semiconductors and magnetic devices.

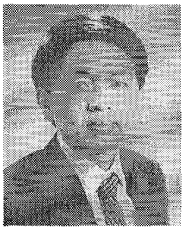

Loc Vu-Quoc received the Diplome d'Ingenieur in structural engineering with highest honors from the Institut National des Science Appliquees, Lyon, France, in 1979. In 1981, he received the M.S. degree in structural mechanics from the Illinois Institute of Technology, Chicago. In 1985 he received the M.S. degree in electrical engineering and computer science, and in 1986 the Ph.D. degree in structural engineering and structural mechanics, both from the University of California at Berkeley.

He worked for two years (1979–1981) developing finite element codes at the Centre Technique des Industries Mechaniques, Senlis, France. He joined the University of Florida in 1988, after two years of post-Doctoral work at Stanford and Berkeley, and is currently an Associate Professor in Aerospace Engineering, Mechanics and Engineering Science. His current research interests are in applied/computational electromagnetics/mechanics, and in power electronics simulation.

Dr. Vu-Quoc received the NSF Presidential Young Investigator award in 1990.